Serial sarcomere number is substantially decreased within the paretic biceps brachii in individuals with chronic hemiparetic stroke

Amy N. Adkins[a,b,c], Julius P. A. Dewald[a,d,e], Lindsay P. Garmirian[a,d,1], Christa M. Nelson[a,d], and Wendy M. Murray[a,b,c,d,e,2]

[a]Department of Biomedical Engineering, Northwestern University, Evanston, IL 60208; [b]Arms + Hands Lab, Shirley Ryan AbilityLab, Chicago, IL 60610; [c]Research Service, Edward Hines, Jr. Veterans Affairs Hospital, Hines, IL 60141; [d]Department of Physical Therapy and Human Movement Sciences, Northwestern University Feinberg School of Medicine, Chicago, IL 60611; and [e]Department of Physical Medicine & Rehabilitation, Northwestern University Feinberg School of Medicine, Chicago, IL 60610

A muscle's structure, or architecture, is indicative of its function and is plastic; changes in input to or use of the muscle alter its architecture. Stroke-induced neural deficits substantially alter both input to and usage of individual muscles. We combined in vivo imaging methods (second-harmonic generation microendoscopy, extended field-of-view ultrasound, and fat-suppression MRI) to quantify functionally meaningful architecture parameters in the biceps brachii of both limbs of individuals with chronic hemiparetic stroke and in age-matched, unimpaired controls. Specifically, serial sarcomere number (SSN) and physiological cross-sectional area (PCSA) were calculated from data collected at three anatomical scales: sarcomere length, fascicle length, and muscle volume. The interlimb differences in SSN and PCSA were significantly larger for stroke participants than for participants without stroke ($P = 0.0126$ and $P = 0.0042$, respectively), suggesting we observed muscle adaptations associated with stroke rather than natural interlimb variability. The paretic biceps brachii had ~8,200 fewer sarcomeres and ~2 cm^2 smaller PCSA on average than the contralateral limb (both $P < 0.0001$). This was manifested by substantially smaller muscle volumes (112 versus 163 cm^3), significantly shorter fascicles (11.0 versus 14.0 cm; $P < 0.0001$), and comparable sarcomere lengths (3.55 versus 3.59 μm; $P = 0.6151$) between limbs. Most notably, this study provides direct evidence of the loss of serial sarcomeres in human muscle observed in a population with neural impairments that lead to disuse and chronically place the affected muscle at a shortened position. This adaptation is consistent with functional consequences (increased passive resistance to elbow extension) that would amplify already problematic, neurally driven motor impairments.

muscle | stroke | sarcomere | fascicle | imaging

Three-fourths of the nearly seven million stroke survivors currently living in the United States report substantial motor impairments that limit their independence in tasks of everyday life (1, 2). Damage to the corticofugal motor pathways and the resulting reliance on indirect corticoreticulospinal pathways following stroke alter neuronal input to contralesional muscles (3–6). Such changes include decreased voluntary neural drive (weakness or paresis) (7, 8) and increased involuntary neural drive (hypertonia), causing the inability to fully activate and fully relax the muscle, respectively. Furthermore, abnormal muscle coactivation patterns (9) also arise from the altered neuronal drive, commonly leading to abnormal limb synergies (10) or a loss of independent joint control (9, 11). For example, in the upper limb, the flexion synergy presents when the individual attempts to abduct their shoulder but involuntarily and concomitantly flexes all of their distal joints (elbow, wrist, and fingers) (9, 12). The flexion synergy limits the ability to combine shoulder abduction and extension of the limb as needed to use

the arm and hand to reach and acquire an object at a distance from the body. Thus, although stroke is primarily an injury of the brain, stroke-induced neural deficits substantially alter input to and use of the contralesional upper limb.

Skeletal muscle is a plastic tissue since changes to both the stimulus it receives and how it is used can alter its functional capacity (e.g., refs. 13 to 19). A muscle's function, its ability to contract and produce force, can be delineated via its architecture (20–23). Specifically, optimal fascicle length (OFL) is the fascicle length at which the muscle generates its maximum force [a fascicle is defined as a bundle of muscle fibers acting in parallel (24)]. OFL is a measure of the number of sarcomeres in series in the muscle, so it also provides a measure of the absolute range of lengths over which the muscle can actively generate force (21, 25). Physiological cross-sectional area (PCSA) is a correlate of the maximum isometric force a muscle can produce given maximum activation (26). These two critical muscle architectural features are calculated from more primary measures of a muscle's

structural anatomy that occur across different scales, including muscle volume, fascicle length, pennation angle (in pennate muscle), and sarcomere length (see *Methods* Eqs. **4** and **5**) (25, 27). Quantifying the adaptation of these two parameters to changes in use and stimulus can provide insight into the functional implications of such changes. For example, a series of classic studies in animal models demonstrate that when limbs were immobilized for an extended time, muscles immobilized at a joint angle that shortened muscle-tendon lengths (i.e., with origin-to-insertion distances that were decreased compared to resting length) lost serial sarcomeres (i.e., adapted such that OFL was shorter) (18, 28–30). Conversely, when immobilized at a joint posture that lengthened muscles, sarcomeres were added in series. These fundamental studies suggest that when in vivo length is chronically altered, a muscle's architecture changes in a way that maximizes its function at the new length. Specifically, in the immobilization studies, the muscle's length "reoptimized" so OFL (the length at which the muscle generates its maximum force) occurred at the joint angle of immobilization.

Despite these important studies, it is unclear the extent to which this mechanism is expressed, in vivo, in human muscle. For example, at this point, only a single published study has calculated serial sarcomere number (i.e., measured both sarcomere length and fascicle length in vivo) under conditions in which a human muscle has chronically been placed at a shortened position (31). In this case, the calf muscles in children with cerebral palsy (CP) with equinus contractures [functionally shortened muscle-tendon units that are more resistant to stretch (32, 33)] severe enough to require surgical intervention did not "reoptimize" to the shorter muscle lengths imposed by the participants' chronically plantarflexed joint posture. Rather, the soleus muscles in these children had sarcomeres substantially longer [4.07 μm (31)] than optimal length [2.70 μm (34)]. Unfortunately, identical measurements could not be collected in a control population because sarcomere length could not be measured in children who were not undergoing surgery. Sarcomere length measurements in living human subjects have traditionally been limited to biopsy or intraoperative studies [i.e., during distraction surgeries for limb discrepancy (13), tendon transfer surgeries (35, 36), or muscle lengthening in children with CP (32)] and only recently have become measurable via minimally or noninvasive techniques (37, 38). As a result, the authors estimated serial sarcomere number for control participants by combining fascicle length measures obtained from typically developing children via ultrasound with sarcomere lengths measured from adult cadavers via dissection. Based on these methods, they concluded the soleus in the children with CP had fewer sarcomeres in series than typically developing muscle (31). This pediatric study suggested that instead of reoptimizing so that OFL occurred at the chronically plantarflexed ankle angle, the shortened muscle shifted to much longer sarcomere lengths at which active force-generating capabilities are weaker, and passive forces are greater.

Stroke-induced neural deficits lead to decreased use and a chronically more flexed resting posture of the paretic upper limb. Given the muscle adaptation observed following immobilization in animal models as well as a general assumption that these type of muscle adaptations do occur in humans with severe neural impairments and may result in muscles that are both structurally weaker and stiffer, there is concern about functional consequences of muscle adaptation following stroke. Thus, several studies have sought to directly quantify in vivo muscle structure in this cohort. In general, in vivo medical imaging has provided strong evidence that many muscle anatomical structural parameters are different in the paretic limb compared to the contralateral limb. Specifically, shorter fascicles (39) as well as smaller pennation angles (40), muscle masses (41), volumes (42, 43), and anatomical cross-sectional areas [the area of muscle perpendicular to the line of action of the external tendons (44)] have been

demonstrated in numerous thigh and shank muscles (42, 45). Similarly, in the upper limb, shorter fascicles (46, 47) and smaller muscle volumes (48) have been reported in various paretic muscles as compared to the contralateral side.

The primary weakness of existing studies that demonstrate differences in anatomical parameters in paretic muscles in chronic stroke is that none also simultaneously measured sarcomere length. Neither OFL nor PCSA is directly calculable in any existing study that describes muscle structure following chronic stroke because they do not report the corresponding measures of both a muscle's sarcomere and fascicle lengths. Thus, insight into how the observed structural differences relate to muscle function in the paretic limb is limited. For example, shorter fascicles in the paretic limb relative to the contralateral limb have been widely demonstrated (39, 46, 47). One explanation of this observation in the elbow flexors could be that they experience conditions similar to muscle immobilization at shortened muscle-tendon lengths; the paretic upper limb is generally used much less than the nonparetic limb, and it rests in a more flexed elbow posture (49). Thus, similar to immobilization studies in animal models (i.e., refs. 18, 28, and 30), shorter fascicles in the paretic elbow flexors could result from a loss of sarcomeres in series. Functionally, this adaptation would indicate a decrease in the absolute range of lengths over which the muscle can generate active force (21). In addition, the animal studies demonstrated that muscles immobilized in a shortened position that had lost sarcomeres in series had passive length–tension curves that were both steeper (increased stiffness) and shifted to shorter fascicle lengths; overall, the muscles that lost sarcomeres in series were described as less "extensible" (30). However, without a concomitant measure of the length of the muscle's sarcomeres, the possibility that fascicle lengths measured in paretic muscle are shorter because there are fewer sarcomeres in series cannot be distinguished from the possibility that the paretic muscle has the same number of sarcomeres in series as in the contralateral limb, but its sarcomeres have adapted by shifting to shorter lengths. In this case, the paretic muscle would be capable of generating active force over the same range of lengths, but the muscle would operate over shorter sarcomere lengths throughout the joint's range of motion. Based on basic muscle physiology, we would expect a muscle operating at shorter sarcomere lengths to generate smaller passive forces throughout the joint's range of motion (44). A single study has reported in vivo measures of biceps brachii sarcomere lengths following chronic hemiparetic stroke (fascicle lengths were not measured); when an individual participant's paretic and nonparetic limbs were positioned in identical limb postures, two of four stroke participants had longer sarcomeres in the paretic biceps, and two had shorter sarcomeres (38). Thus, the implications for OFL, the range of lengths over which the muscle can generate active force, and the passive forces the muscle produces over the joint's range of motion remain unclear. These distinct possibilities for sarcomere adaptation would also have different effects on maximum isometric force capacity. While a decrease in muscle volume is regularly reported in paretic limbs (42, 48), PCSA is the architectural correlate of force-generating capacity, and it is calculated using the ratio between muscle volume and OFL. Critically, stroke alters both neural input to (5–7) and use of (8, 9, 11, 12) the paretic limb. Thus, it is also possible that paretic muscle adapts in an unexpected manner poststroke; animal models of immobilization limited the use of the limb and altered muscle length but did not involve neural injury.

In this study, we quantify multiscale muscle parameter differences, in vivo, in the biceps brachii of the paretic and contralateral limbs of individuals with chronic hemiparetic stroke and in both limbs of a group of age-matched individuals with no history of musculoskeletal or neurological diseases or injuries to the upper limb. Specifically, sarcomere length, fascicle length,

and muscle volume are measured from images obtained using second-harmonic generation microendoscopy, extended field-of-view ultrasound, and fat-suppression magnetic resonance imaging, respectively. Our key finding was that the paretic biceps of individuals with chronic hemiparetic stroke have fewer sarcomeres in series (i.e., shorter OFL) compared to the contralateral muscle; interlimb difference in serial sarcomere number was significantly greater than for participants without stroke ($P = 0.0126$). In the limb posture we evaluated, this result was manifested by systematically shorter fascicles without an observable effect for average sarcomere length in the paretic muscle relative to the nonparetic, contralateral biceps. Our data provide direct evidence of muscle adaptation involving the loss of serial sarcomeres in living human subjects and is observed in a population with neural impairments that chronically place the affected muscle at a shortened position. This muscle architectural difference post chronic hemiparetic stroke is consistent with functional consequences that would amplify the already problematic neural driven motor impairments (i.e., the ability to reach away from the body to grab an object).

Results

Serial Sarcomere Number, Fascicle Length, and Sarcomere Length. Relative to the contralateral, nonparetic limb, the paretic biceps brachii of individuals in this study with chronic hemiparetic stroke had fewer sarcomeres in series; a comparable interlimb difference was not observed in participants without stroke. The within-subject interlimb differences were significantly larger in the stroke group than the nonstroke group ($P = 0.0126$). Specifically, interlimb difference in serial sarcomere number (SSN) for the stroke participants was 8,178 (95% CI: 4,082 to 12,274; $P < 0.0001$) compared to −478 (95% CI: −5,900 to 4,945; $P = 0.8628$) for the participants without stroke. The general linear mixed-effects model (GLMM) indicated the mean SSN in the paretic muscle was 31,335 (95% CI: 27,646 to 35,024) compared to 39,513 (95% CI: 35,824 to 43,202) in the nonparetic muscle (cf., black circles and SE bars, Fig. 1). In contrast, in the four participants who did not have a stroke, biceps SSN was comparable between dominant (39,527, 95% CI: 34,646 to 44,409) and nondominant limbs (40,005, 95% CI: 35,122 to 44,888). The achieved effect size (Cohen's d, interlimb differences between groups), calculated from the data (cf., colored symbols, Fig. 1), was 1.784.

In these participants, at the single joint posture we tested, interlimb differences in biceps fascicle lengths in the stroke group were also significantly larger than in the group without stroke ($P = 0.0030$; Cohen's $d = 2.159$; Fig. 2). There was a significant difference (3.03 cm; 95% CI: 1.91 to 4.14 cm) in fascicle length between the paretic (11.00 cm; 95% CI: 10.12 to 11.89 cm) and nonparetic (14.03 cm; 95% CI: 13.15 to 14.91 cm) limbs in the stroke group ($P < 0.0001$, Fig. 2A). Notably, the differences in fascicle length between the paretic and nonparetic limbs cannot be explained by interlimb differences in humerus length (Table 1). In contrast to SSN and fascicle length, within-subject interlimb differences in sarcomere length were not significantly different between the stroke and control groups ($P = 0.6791$; Cohen's $d = −0.280$; Fig. 2B). Notably, the achieved effect sizes for interlimb differences in SSN and fascicle length are six to eight times larger than for sarcomere length in these 11 participants (stroke versus control).

PCSA and Muscle Volume. Overall, the interlimb difference in muscle volume for the stroke participants included in this study was significantly larger than for the participants without stroke ($P = 0.0082$; Cohen's $d = 2.188$; Fig. 3A). Specifically, the median interlimb difference in muscle volume in the seven participants who had experienced a stroke (42.67 cm³, quartile range: 23.54 cm³) was significantly larger than the median interlimb difference in the four participants without stroke (0.48 cm³, quartile range: 7.65 cm³). The interlimb difference in PCSA was
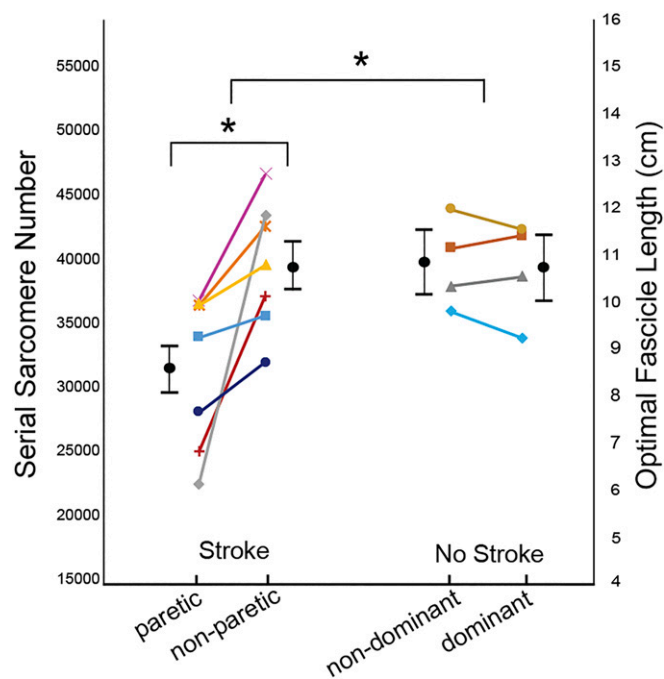

Fig. 1. SSN/OFL. Data illustrating interlimb differences in SSN and, proportionally, OFL for all participants who had a stroke and the age-range matched controls (no stroke). The average of the calculated parameter value (see Eqs. **4** and **5**) for each individual participant is represented by a symbol of different shape/color, and each individual's limbs are connected by a line. Black filled circles and error bars which are offset from individual participant data represent mean and SE estimated from the GLMM. The asterisk (*) indicates a significant difference ($P < 0.05$).

also significantly larger in the participants who had undergone a stroke (1.98 cm²; 95% CI: 1.19 to 2.77 cm²; $P < 0.0001$) than for those without stroke (0.06 cm², 95% CI, −0.99 to 1.11 cm²; $P = 0.9061$). The GLMM indicated the mean PCSA in the paretic muscle was 13.09 cm² (95% CI: 9.10 to 17.08 cm²) compared to 15.07 cm² (95% CI: 11.08 to 19.06 cm²) in the nonparetic muscle (Fig. 3B). In the four participants who did not have a stroke, biceps PCSA was comparable between dominant (11.49 cm²; 95% CI: 6.22 to 16.77 cm²) and nondominant limbs (11.43 cm²; 95% CI: 6.12 to 16.71 cm²; Fig. 3B). Despite the significant interlimb difference in PCSA in the participants with stroke, normalized interlimb differences in PCSA (15.6%) were smaller than those in volume (32.7%) due to fewer sarcomeres in series (Fig. 4).

Discussion

This study aimed to compare in vivo muscle architecture parameters in individuals with chronic hemiparetic stroke and individuals who had not undergone a stroke. For our primary outcome measure (interlimb differences in parameters observed between the groups of participants with and without stroke), the observed effects for interlimb differences in SSN (Cohen's $d = 1.784$), fascicle length (Cohen's $d = 2.159$), muscle volume (Cohen's $d = 2.188$), and PCSA (Cohen's $d = 2.019$) were large and substantially greater than those for sarcomere length (Cohen's $d = −0.280$) in these 11 participants. Most notably, we found significantly fewer sarcomeres in series in the paretic muscle compared to the contralateral side with an interlimb difference that was significantly greater than in the participants without stroke. In all seven participants with stroke included in this study, we observed strikingly smaller muscle volumes on the paretic side (Fig. 4). While a difference in muscle volume (area × length) is often considered synonymous with a difference in

Adkins et al.
Serial sarcomere number is substantially decreased within the paretic biceps brachii in individuals with chronic hemiparetic stroke

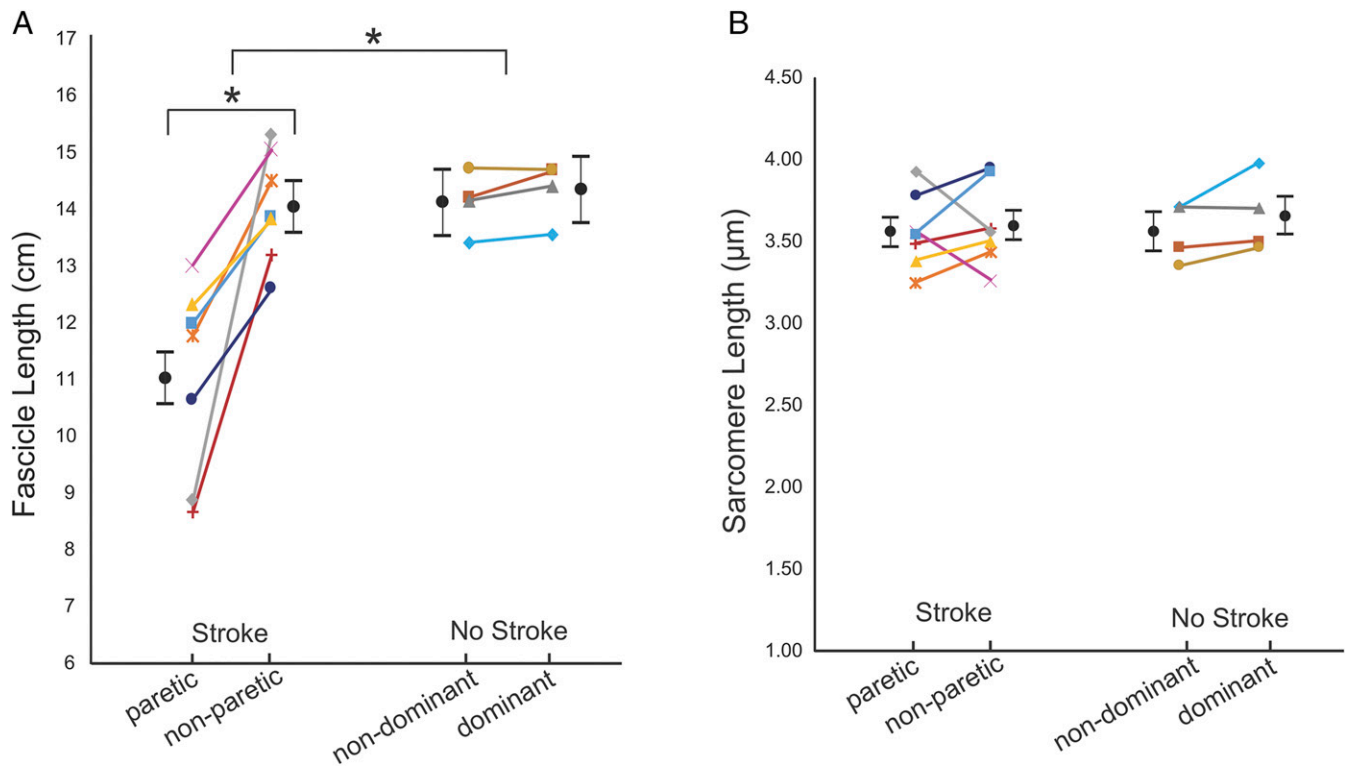PNAS | 3 of 10
https://doi.org/10.1073/pnas.2008597118

Fig. 2. Fascicle and sarcomere length. Average fascicle length (*A*) and sarcomere length (*B*) measurements from both limbs and in all participants in the stroke and control (no stroke) groups. The average of the measured parameter values for each individual participant is represented by a symbol of different shape and or color. Each individual's limbs are connected by a solid line. Black filled circles and error bars which are offset from individual participant data represent mean and SEs estimated from the GLMM. The asterisk (*) indicates a significant difference ($P < 0.05$).

PCSA (i.e., refs. 42 and 50 to 52), our data suggest that the differences in muscle volumes we observed between limbs in the participants with stroke were not actually a direct measure of the differences in maximum isometric force-generating capacity (under conditions of full activation) due to the loss of sarcomeres in series (Fig. 4). Shorter OFL indicate a proportional decrease in the width of the muscle's isometric force–length curve (22, 24, 44) or—more explicitly—a proportional decrease in the absolute range of lengths over which the muscle can generate active force.

The substantial decrease in SSN that occurs when a muscle is held at a joint posture which places it at a shortened length was first reported in classic limb immobilization studies in animal models (18, 28, 30); it is widely assumed to be a fundamental muscle adaptation process. We now provide direct evidence of this phenomenon in living human study participants.

The most complete demonstration of in vivo muscle adaptation that accompanies chronic length changes has been via animal models involving limb immobilization (18, 28–30). The main

Table 1. Participant demographic information

	Gender	Age*	Paretic	Bone length (cm) paretic	Bone length (cm) nonparetic	Years poststroke*	Fugl-Meyer Assessment
1	F	65	R	31.3	31.0	32	15
2	F	63	L	29.5	30.2	15	24
3	M	48	L	32.6	32.6	8	38
4	M	60	R	29.2	30.0	7	18
5	M	72	R	30.8	30.1	22	15
6	M	62	L	30.5	32.0	5	47
7	M	44	R	32.9	33.1	5	39
Average(SD)	59(10)	—		31.0(1.4)	31.3(1.3)	13(10)	28(13)

	Gender	Age*	Dominant	Bone length (cm) nondominant	Bone length (cm) dominant
8	F	53	R	29.9	29.7
9	F	64	R	29.7	29.5
10	M	62	R	36.4	35.3
11	M	67	R	32.4	31.5
Average(SD)	62(6)	—		32.1(3.1)	31.5(2.7)

*Age for all participants and years poststroke for participants with stroke (subjects one to seven) are reported as of the time at which the experimental data collection for that participant was completed.
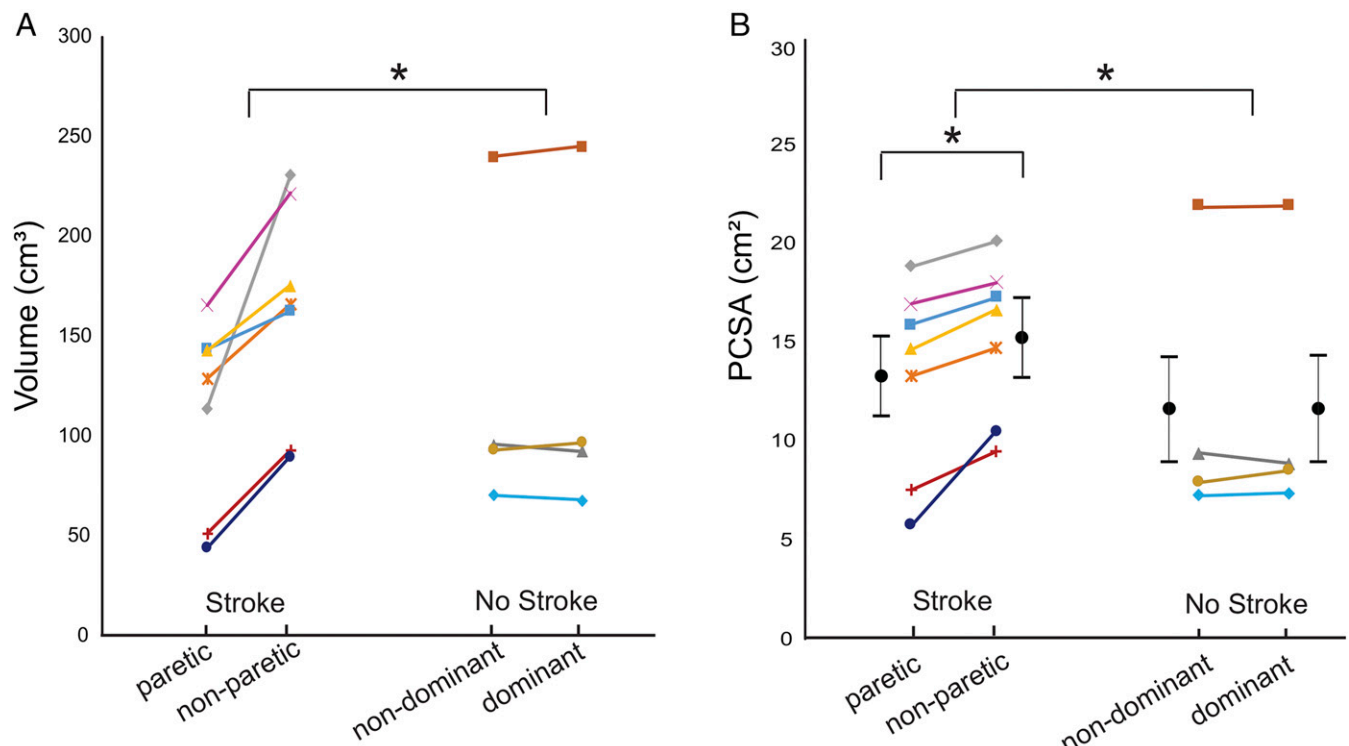
Fig. 3. Muscle volume and PCSA. Biceps brachii muscle volume (with intramuscular fat removed) (*A*) and calculated PCSA (see Eq. **6**) (*B*) for both limbs of all participants who had a stroke and the age-matched controls (no stroke). The average of the parameter values for each individual participant is represented by a symbol of different shape and or color. Each individual's limbs are connected by a solid line. Black filled circles and error bars which are offset from individual participant data represent mean and SE estimated of PCSA from the GLMM. In *A*, the asterisk (*) indicates a significant difference in muscle volume across groups (stroke versus no stroke) established from implementing the Mann–Whitney *U* test ($P < 0.05$). In *B*, the asterisk (*) indicates a significant difference either across (stroke versus no stroke) or within groups (i.e., paretic versus nonparetic) in PCSA estimated from the GLMM ($P < 0.05$).

difference between the adaptations observed in our study compared to these studies of limb immobilization is the magnitude of the observed adaptation. The decrease in SSN we observed in the paretic biceps poststroke was less substantial than the loss of serial sarcomeres observed following immobilization at a shortened muscle-tendon length in animal models (∼20 versus ∼40%). The
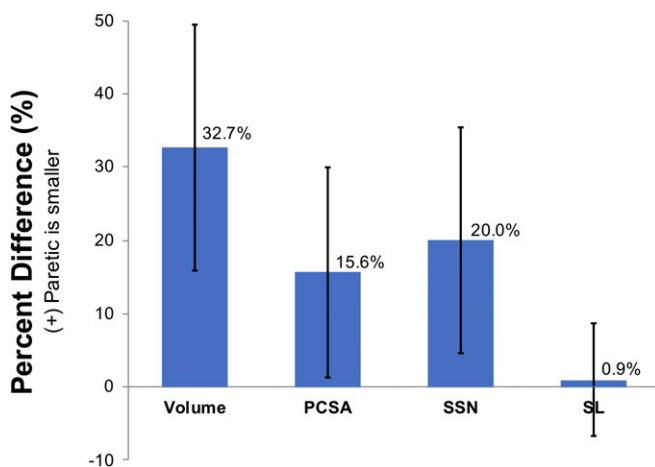

Fig. 4. Interlimb muscle differences poststroke. Average percent difference in muscle architectural parameters, including muscle volume, PCSA, SSN, and sarcomere length (SL) was calculated for all participants included in our study who had experienced a stroke and had smaller muscle volume on the paretic biceps. A positive percent difference indicates that the paretic parameter is smaller than the nonparetic side. Error bars represent one SD from the mean of the percent difference across the subjects.

prime difference between individuals poststroke and animal immobilization studies, which may explain this difference in magnitude, is that poststroke individuals tend to disuse their paretic limb but still have active and passive joint motion, whereas animal immobilization studies eliminated movement entirely. In our stroke participants, the studied muscle also receives altered neural inputs; the animal studies did not involve a supraspinal neural injury.

Intraoperative measures of sarcomeres have been shown to be much longer in children with CP than sarcomere length estimates for (31) or intraoperative measures (32) in typically developing children. In contrast, our data indicate that the effect of stroke on interlimb differences in sarcomere length was relatively small in these adult participants, with absolute sarcomere length measures comparable to the participants without stroke (Fig. 2*B*). We expect that a critically important difference between muscle adaptation following stroke and CP is that stroke occurs in a fully developed system. Similar to the biceps brachii in our population, the affected muscles in the CP studies were chronically in a shortened positioned due to the primary neural impairments. However, it has been posited that while chronically shortened CP muscle loses sarcomeres in series as would be expected from the classic immobilization studies, a malfunctioning sensing system within the muscles prevents the addition of serial sarcomeres during bone growth, resulting in the abnormally long sarcomeres (32). Thus, the additional physiological process of bone growth in children with CP confounds direct comparison with muscle adaptation that occurs in adults with stroke.

In general, our work provides the most direct confirmation in humans to date that chronic impairments that lead to disuse and place a muscle in a shortened position are associated with the loss of serial sarcomeres. In the context of the literature discussed in the paragraph above, we note that this adaptation

Adkins et al.
Serial sarcomere number is substantially decreased within the paretic biceps brachii in individuals with chronic hemiparetic stroke

process also seems to be moderated by the presence of other factors (i.e., bone growth [CP], altered neural input, disuse resulting in a reduced use of available range of motion, etc.). Such factors are common in vivo following disease, neural injury, and clinical interventions such as surgery or immobilization. With the comprehensive multiscale imaging techniques utilized in this study, adaptation of muscle structure in the context of these factors can now be better explored and more fully understood in humans, which is necessary for the development of more targeted interventions that seek to improve outcomes.

The substantial decrease in SSN found in the paretic biceps brachii likely amplifies motor impairments which stem from stroke-induced neural impairment. Decreased voluntary neural drive (weakness or paresis) (7, 8), increased involuntary neural drive (hypertonia), and abnormal muscle coactivation patterns (9) occur following damage of the corticofugal motor pathways because of a stroke. In addition, it is clear that the stroke-induced neural deficits result in altered use of the contralesional or paretic limbs. Particularly notable is the difficulty (and in severe cases impossibility) of coordinated extension of the upper limb to reach and grab an object which is some distance from the body (12, 53). In this study, we find that the muscle structure itself is different, with fewer serial sarcomeres in the paretic biceps brachii muscle. Functionally, for the individuals in our study who had survived a stroke, this means that the paretic muscle has a narrower range of lengths and joint angles over which it can produce active force. The loss of sarcomeres in series would also imply a shift of the passive length–tension curve to shorter fascicle lengths (30), which would correspond to the onset of passive elbow torques in more flexed postures. Notably, animal muscles immobilized in a shortened position also exhibited steeper (stiffer) passive length–tension curves (30). Similarly, muscle biopsies from pediatric patients with CP demonstrate the extracellular matrix contributes to increased passive muscle stiffness (54). Thus, we expect the loss of serial sarcomeres that we observed may also be accompanied by a number of physiological changes in the muscle that, together, ultimately result in increased passive muscle stiffness beyond a simple shift in the length of onset. Especially because elbow extensor weakness is a common sequelae of chronic hemiparetic stroke (55), all of these factors could exacerbate the neurally driven motor impairments that diminish the ability to extend the elbow to reach for an object away from their body.

Our study reports in vivo PCSA calculated from direct measures of all critical architectural parameters (fascicle length, muscle volume, and sarcomere length for a fusiform muscle). Prior studies reporting in vivo PCSA have done so using medical imaging methods to obtain measures of volume and fascicle length (40, 56–59), yielding indirect estimates of PCSA (because sarcomere length was not measured). The inclusion of sarcomere length in the calculation of PCSA is critical. For example, using the measurements made in our study, an indirect estimate of PCSA (volume divided by fascicle length, 9.99 cm^2) would underestimate average PCSA (volume divided by optimal fascicle length, 13.08 cm^2) in our study by 24%. Musculoskeletal models have been shown to have difficulty estimating realistic muscle forces using currently available muscle architectural parameters. To correct for this, modeling studies use specific tension values [i.e., 45 to 140 N/cm^2 (60), 60 N/cm^2 (61)] much larger than values determined experimentally in single-fiber studies in animal muscle (~22.5 N/cm^2; i.e., refs. 62 and 63). The absence of direct measures of PCSA in vivo may contribute to this difficulty.

The results from our study are reasonable in the context of previously reported in vivo studies which independently measure either fascicle length, muscle volume, or sarcomere length. Specifically, muscle fascicle lengths in the paretic biceps brachii in this study were on average 21.4% shorter than the nonparetic side. Previous studies performed in elbow flexors report similar

substantial decreases in fascicle length in extended joint postures [18.6% decrease in biceps brachii at 25° elbow flexion (47), and 15% decrease in brachialis at 10° elbow flexion (46)]. The studies of muscle volume differences between paretic and nonparetic limbs are variable. On average, our muscle volume differences (32.7%) are in the same direction (paretic muscle is smaller) and of slightly greater magnitude than other upper limb studies [no difference to 25% difference (41, 48)] and lie within the range of lower limb differences [no difference to 33% difference (35, 49)]. The range of healthy muscle volumes in our study—including both arms of the unimpaired individuals and the nonparetic arm of individuals with chronic hemiparetic stroke (66 to 247 cm^3)—is reasonable within the context of other in vivo muscle volume studies of the biceps brachii in healthy individuals (76 to 266 cm^3) (50, 64). The exclusion of intramuscular fat in our measure of muscle volume may explain our slightly higher percent differences and slightly smaller muscle volumes. The measurements of biceps brachii sarcomere lengths have only been obtained in vivo in a single study that enrolled four individuals with chronic hemiparetic stroke. Similar to this previous work, we observed some individuals with shorter sarcomeres in their paretic limb, while others had longer (38). Notably, independently measured muscle anatomical parameters (particularly sarcomere lengths and nonnormalized fascicle lengths) are difficult to directly compare between studies, as they are sensitive to the limb posture chosen for testing (65); muscle fascicle and sarcomere lengths change with joint position.

There are a number of limitations to this study that should be considered. In particular, while our main conclusions are accompanied by large effects, the relatively small cohort of individuals we evaluated limited our ability to make statistically robust conclusions for some muscle architecture parameters (especially sarcomere length) because of the smaller effect sizes observed between groups in these participants. In addition, our findings and their implication for muscle adaptation post–brain injury would be strengthened if future work evaluated additional muscles (beyond the biceps brachii), tested in multiple joint positions, and included factors that quantify the extent participants use their upper limbs (i.e., passive and active range of motion, elbow joint resting posture, amount of voluntary use of limb, etc.). We would expect that altered tendon properties or increased tendon length (66) could accompany the paretic muscle adaptation we observed, but we did not include these measures in this study. Similarly, we did not quantify active muscle function (e.g., ref. 55), passive joint stiffness (e.g., refs. 9 and 67), or changes in muscle or tendon material properties (e.g., ref. 68). Linking the data we report here to measures of muscle function is needed to elucidate muscle-tendon adaptation poststroke.

Beyond the addition of comprehensive measurements of in vivo muscle architecture for the investigation of muscle plasticity to stroke-induced neural deficits, this study demonstrates the need for such work and provides insight for the design of therapeutic interventions for stroke survivors. The combination of measures of muscle volume with both fascicle and sarcomere lengths that were measured at the same limb position reduces the ambiguity associated with interpreting these same parameters if they were measured in isolation. Many prior studies in stroke and other populations demonstrate interlimb differences in fascicle length without normalizing to sarcomere length. With the addition of sarcomere length, we were able to explicitly demonstrate that the paretic biceps brachii muscle has fewer serial sarcomeres. Our finding leads us to conclude that stroke-induced neural deficits, which lead to altered input and disuse of the contralesional limb, ultimately change the basic biceps brachii muscle architectural parameters in a way which may amplify functional impairments.

Methods

Participants. The measurements of sarcomere length, fascicle length, and muscle volume of the biceps brachii were obtained using in vivo imaging techniques in both arms of 12 participants; eight participants with chronic hemiparetic stroke (three female/five male, 60 ± 9 y, Fugl-Meyer 26 ± 9, 13 ± 10 y poststroke) and four participants with no history of musculoskeletal or neurological diseases or injuries to the upper limb (two female/two male, 62 ± 6 y). One of the eight individuals with chronic hemiparetic stroke was retrospectively removed due to the discovery that the individual had sustained a rotator cuff tear in the nonparetic shoulder, which was unknown to us at the time of recruitment and data collection. Fugl-Meyer assessment scores reported in this study were performed by a licensed physical therapist prior to experimentation. All the individuals who participated in this study provided informed consent prior to experimentation; Northwestern University's Institutional Review Board approved this study's procedures. Data from this study can be accessed through Northwestern's Arch, an open access repository for research and data (https://doi.org/10.21985/n2-anqa-xq41).

Sarcomere Length. Sarcomere lengths of both arms were acquired with the participants seated in a comfortable chair. The arm being imaged was secured at 85° shoulder adduction, 10° horizontal shoulder flexion, 25° of elbow flexion, mid-prosupination, and 0° wrist and finger flexion (Fig. 5). Joint posture was verified by goniometric measurement. A microendoscopic system (Zebrascope, Enspectra Health), which consists of a laser (class IV, output power > 500 mW, center wavelength 1,030 nm), microscope, and microendoscopic probe, was used to image sarcomeres in vivo. This system utilizes the second-harmonic generation optical technique to capture the intrinsic striation pattern of sarcomeres (37, 38).

A sterile microendoscopic probe was inserted into the long head of the biceps brachii. The probe consisted of two 1.8-cm long, 20-gauge needles with beveled tips (Fig. 5B), one needle with a transmitting lens used to excite the muscle tissue and one needle housing a receiving lens to capture the reflection of the signal after it has interacted with tissue. Ultrasound and palpation techniques were used, prior to insertion, to verify the placement of the probe at mid-belly of the muscle with the probe's optical lenses aligned parallel to the fascicle direction. A spring-loaded injector was used to rapidly insert the probe, minimizing pain and improving precision of probe placement. The microscope was attached to the microendoscopic

needle for imaging. Images with a field-of-view of 82 by 82 μm were collected at 1.9 Hz for ~2 to 5 min. The image produced from the microendoscopic system captures the A-bands (myosin protein) of the sarcomeres and enables direct measurement of sarcomeres from the resulting striation pattern (38). The surface electromyogram (EMG; Bagnoli-16 system, Delsys, Inc.) of the biceps brachii was obtained simultaneously using a custom-written MATLAB script. Baseline EMG activity was collected for 10 s with the needle inserted and participant relaxed. Muscle activation was visually monitored during data collection, and analysis was performed offline.

Fascicle Length. Fascicle length measurements of the long head of the biceps brachii in both arms of all participants were obtained using extended field-of-view ultrasound (EFOV-US) under the same conditions (same joint posture, passive muscle) as sarcomere length measures. The extended field-of-view technique involves sweeping the ultrasound probe along the length of the muscle as sequential B-mode ultrasound images are acquired and stitched together to form a single composite image with a field-of-view longer than the ultrasound probe's aperture (±60 cm) (69). This method has been demonstrated to be accurate and reliable for measurement of fascicle length in different individuals and muscles (65, 70). Approximately 10 qualitatively good images were captured per arm. EFOV-US images (Acuson S2000, linear array transducer 18L6, SieScape, Siemens Medical Solutions USA, Inc.) and surface EMG (Bagnoli-16 system, Delsys Inc.) of the biceps brachii were simultaneously recorded (Spike, Power1401, and Micro1401-3, Cambridge Electronic Design Limited).

Muscle Volume. To determine the volume of the biceps brachii muscle excluding intramuscular fat, the Dixon method, a fat-suppression MRI sequence, was implemented on both upper limbs of all participants (three-dimensional [3D] dual-echo gradient, repetition time [TR] = 7 ms, flip angle = 12°, matrix size = 256 × 304, slice thickness = 3 mm, echo time [TE] of 2.45 and 3.68 ms) (48). As increases in intramuscular fat within muscle has been demonstrated in the lower limb of stroke participants (42) and patients with other pathologies [i.e., whiplash (71), spinal cord injury (72)], correcting muscle volumes for the amount of intramuscular fat is necessary to avoid potential overestimation of volume of muscle. The participants were lying supine in a 3T MRI (Area, Siemens Medical Solutions USA, Inc.) scanner with their arm as close to the center of the scanner as possible. To minimize participant movement during scanning, the lower arm was splinted using an orthosis.
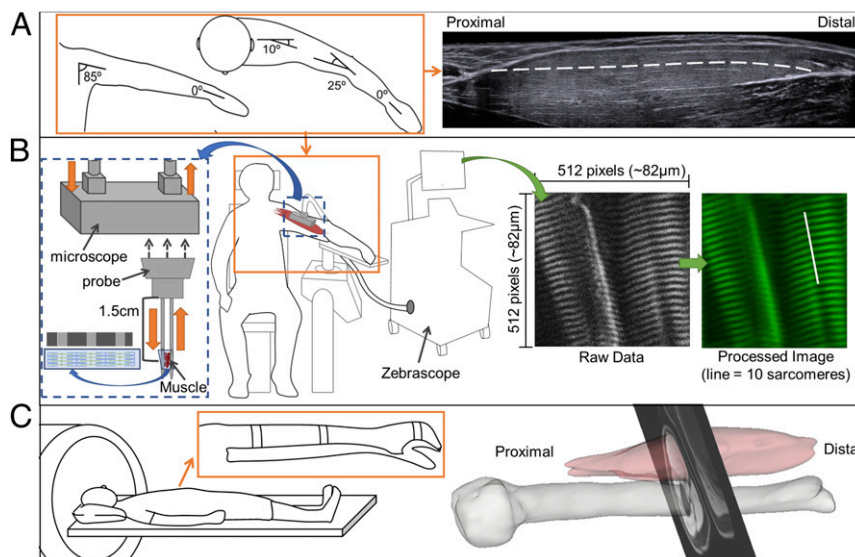
Fig. 5. Illustration of experimental set up for muscle architecture measures. (*A*) Arm posture used for measurement of fascicle length using ultrasound (*Right*) and for sarcomere length (see *B*). The white dashed line overlaid on the ultrasound image illustrates a manually segmented muscle fascicle. (*B*) Illustration of the experimental setup for the Zebrascope, which utilizes second-harmonic generation microendoscopy to capture the natural striation pattern of sarcomeres in vivo. The Biodex chair and arm fixture (*Middle*) was used for both measurements of sarcomere and fascicle lengths (see *A*). The microscope is enlarged on the left (blue dashed box) to depict the flow of laser light through the microscope (orange arrows). Below the microscope is a graphic of the probe that is inserted into the muscle. The laser light interacts with myofibrils between the two needles at a location of 1.5 cm from the base of the probe. To the right, a raw image which would be seen during image collection and the same image after postprocessing are shown. Sarcomere length is measured from the processed image; for reference, the length of 10 sarcomeres in series are indicated by a white line. (*C*) Participant in the supine positioning (*Left*) in the MRI bore. (*Inset*) The splinting of the arm to reduce artifacts because of hand and arm movement. (*Right*) 3D rendering of the biceps brachii muscle and humerus bone with a single MRI slice superimposed.

Adkins et al.
Serial sarcomere number is substantially decreased within the paretic biceps brachii in individuals with chronic hemiparetic stroke

www.manaraa.com

Data Analysis.

Sarcomere length. Image sequences obtained from the microendoscopic system were postprocessed offline using a script provided with the ZebraScope by Enspectra Health (previously Zebra Medical Technologies). With this script, the raw image sequence was first combined into a multipage Tiff. Then, a fast Fourier transform (FFT) cleared the edges and vertical center which contained only noise; the transformed data were symmetrically low-pass Gaussian filtered. Within the script, we set the frequency bounds to remove all images without sarcomeres from the multipage Tiff sequence. White noise in the FFT was calculated and removed. To determine mean sarcomere length from each processed image, the peak frequency of a least squares fit of a Gaussian was calculated. The final outputs of the image processing script for each arm and each participant were mean sarcomere length and SD, calculated using all processed images that were not excluded by the specified frequency bounds. At this point, we used our own custom-written MATLAB code to further exclude images that were collected when the biceps EMG signal was 3 SDs above the resting baseline EMG. Thus, the mean sarcomere lengths and SDs that we report for each biceps brachii were calculated from the processed image data, further restricted by the synced EMG data to only include images that were collected under passive conditions. In a single arm of one participant with stroke (the nonparetic arm of participant three), the EMG activity during the Zebrascope trial exceeded the threshold of 3 SDs above the resting baseline EMG. However, when the trial EMG for this single arm was normalized to maximum voluntary contractions (MVCs), the level of EMG activity remained consistently low (mean ± SD: 2.9 ± 3.0% of MVC) throughout the trial. Therefore, we included the sarcomere length data collected from this arm in our analysis. Sarcomere length distributions per subject can be found in *SI Appendix*, Fig. S1.

Fascicle length. EFOV-US images were exported as Digital Imaging and Communications in Medicine (DICOM) images, and measurements of fascicle length were made offline using the segmented line tool in ImageJ [ImageJ with Fiji, version 1.51 h, Wayne Rasband, NIH (73)]. Measurements were made on three images per arm per participant. The experimenter selected the three images which best captured the entire muscle and had visible fascicles which extended from central tendon to aponeurosis. Four fascicles were measured per image. Fascicles were measured in the superficial portion of the muscle where the image quality better allowed for fascicle visualization. Mean fascicle length was calculated across the three images (3 images × 4 fascicles per image = 12 fascicles) (47, 65). The reliability of fascicle length measurements in this study was found to be high (intraclass correlation coefficient [ICC] 0.982 95% CI 0.949 to 0.994) as assessed by blinding a small subset of images to condition (arm, subject) 9 mo after the original measurement and computing a one-way random ICC.

Muscle volume. A manual segmentation of the biceps brachii (long and short heads) muscle was performed using Analyze12.0 (AnalyzeDirect). To calculate the volume of muscle without intramuscular fat (V_{m-f}), the following equations were implemented:

$$\% \, Fat = \frac{intensity \, of \, fat}{intensity \, of \, water \, + \, intensity \, of \, fat}, \quad [1]$$

$$V_{intramuscular \atop fat} = V_{total} * \% \, Fat, \quad [2]$$

and

$$V_{m-f} = V_{total} - V_{intramuscular \atop fat}, \quad [3]$$

in which V_{total} is the total volume segmented from the MRI images, "*intensity of fat*" is the mean pixel intensity from the fat-only image created when using the Dixon technique, and the "*intensity of water*" is the mean pixel intensity from the water-only image created when using the Dixon technique (similar to refs. 48, 74, and 75). The measurements of biceps muscle volume without fat were made by two different raters (rater one $n = 6$, rater two $n = 5$). The segmentation and calculation of muscle volume without intramuscular fat (V_{m-f}) has been shown to be reliable within and across raters (48).

Calculation of Functional Parameters.

With the quantification of sarcomere length, fascicle length, and muscle volume, OFL, SSN, and PCSA were calculated for both arms of all participants using the following equations:

$$SSN = \frac{l^F}{l^S}, \quad [4]$$

$$OFL = SSN * l_o^S, \quad [5]$$

and

$$PCSA = \frac{V_{m-f}}{OFL}, \quad [6]$$

in which l_o^S is 2.7 μm, or optimal sarcomere length (34), and l^F (fascicle length), l^S (sarcomere length), and V_{m-f} (volume of muscle without fat infiltration) were measured in this study. For statistical analysis involving Eqs. **4–6**, average fascicle length and all measures of sarcomere length were utilized.

Bone Length.

As a measure of participant size, humerus length was quantified for all participants (Table 1). To measure bone length, we manually segmented the humerus of each limb from the same images used to compute muscle volume in the same software environment. The rendered volume was then exported to SolidWorks, where length was calculated along the longitudinal axis of the bone.

Statistical Analysis.

For the primary comparison of interest, we compared the interlimb differences observed in the stroke participants to those observed in the participants without stroke for each measured and computed muscle architecture parameter. GLMMs were implemented (SAS 9.4, SAS Institute, Inc.) for each parameter except muscle volume. For the analyses of interlimb differences with GLMMs, each outcome of interest (i.e., SSN, fascicle length, etc.) was the outcome variable for a separate model. The fixed effects included group (whether or not the participant had a stroke), arm (paretic/nondominant versus nonparetic/dominant), and a group × arm interaction. Subject random effect was included in the model to account for the within-subject correlation between arms. An arm-within-subject random effect was also included to account for the within-arm correlation between multiple measurements on the same arm. Muscle volume only yielded a single measurement per arm; this mixed-effects model only included a subject random effect. However, because the model residuals did not satisfy the normality assumption, a Mann–Whitney *U* test was used to compare the within-subject interlimb differences in biceps volume between the stroke participants and the control participants. Using the GLMMs, we also report model-based estimates and secondary comparisons within stroke and control groups. Mean, SE, and 95% CIs are presented in the results for all GLMM estimates. Across all analyses, $P < 0.05$ was considered statistically significant.

An a priori power analysis was conducted to determine sufficient sample size to test the hypothesis that participants with stroke have interlimb differences in SSN that are greater than in individuals who have not had a stroke. The analysis indicated that with eight participants with stroke and four participants without stroke and a standardized effect size (Cohen's *d*) greater than 1.85, a power greater than 0.8 would be achieved at a significance level α = 0.05. An appropriate effect size was established based on interlimb differences in fascicle lengths (46) and sarcomere lengths (49) measured in separate populations but that included data from both arms in both stroke and control participants. Finally, we calculated the Cohen's *d* effect size achieved for each muscle architecture parameter using the data collected to provide context for our statistical findings.

Data Availability.

All measured muscle architecture parameters (sarcomere length, fascicle length, muscle volume) have been deposited in Arch, Northwestern University Research and Data Repository (DOI: 10.21985/n2-anqa-xq41).

De-identified raw second harmonic generation images, raw ultrasound images, and the 3D surface reconstructions of the biceps brachii and humerus created by manually segmenting MRI images have been deposited in Arch. In addition, the repository includes the custom MATLAB codes associated with processing raw sarcomere images and the SAS code used for statistical analysis.

8 of 10 | **PNAS**
https://doi.org/10.1073/pnas.2008597118

Adkins et al.
Serial sarcomere number is substantially decreased within the paretic biceps brachii in individuals with www.manaraa.com

1. E. J. Benjamin et al.; American Heart Association Council on Epidemiology and Prevention Statistics Committee and Stroke Statistics Subcommittee, Heart disease and stroke statistics-2019 update: A report from the American Heart Association. *Circulation* 139, e56–e528 (2019).
2. I. Faria-Fortini, S. M. Michaelsen, J. G. Cassiano, L. F. Teixeira-Salmela, Upper extremity function in stroke subjects: Relationships between the international classification of functioning, disability, and health domains. *J. Hand Ther.* 24, 257–264, quiz 265 (2011).
3. M. D. Ellis, J. Drogos, C. Carmona, T. Keller, J. P. Dewald, Neck rotation modulates flexion synergy torques, indicating an ipsilateral reticulospinal source for impairment in stroke. *J. Neurophysiol.* 108, 3096–3104 (2012).
4. B. Zaaimi, S. A. Edgley, D. S. Soteropoulos, S. N. Baker, Changes in descending motor pathway connectivity after corticospinal tract lesion in macaque monkey. *Brain* 135, 2277–2289 (2012).
5. H. Karbasforoushan, J. Cohen-Adad, J. P. A. Dewald, Brainstem and spinal cord MRI identifies altered sensorimotor pathways post-stroke. *Nat. Commun.* 10, 3524 (2019).
6. J. G. McPherson et al., Progressive recruitment of contralesional cortico-reticulospinal pathways drives motor impairment post stroke. *J. Physiol.* 596, 1211–1225 (2018).
7. D. Bourbonnais, S. Vanden Noven, Weakness in patients with hemiparesis. *Am. J. Occup. Ther.* 43, 313–319 (1989).
8. G. Carin-Levy et al., Longitudinal changes in muscle strength and mass after acute stroke. *Cerebrovasc. Dis.* 21, 201–207 (2006).
9. J. P. Dewald, P. S. Pope, J. D. Given, T. S. Buchanan, W. Z. Rymer, Abnormal muscle coactivation patterns during isometric torque generation at the elbow and shoulder in hemiparetic subjects. *Brain* 118, 495–510 (1995).
10. S. Brunnstrom, *Movement Therapy in Hemiplegia: A Neurophysiological Approach* (Harper & Row, New York, NY, ed. 1, 1970).
11. L. C. Miller, J. P. A. Dewald, Involuntary paretic wrist/finger flexion forces and EMG increase with shoulder abduction load in individuals with chronic stroke. *Clin. Neurophysiol.* 123, 1216–1225 (2012).
12. T. M. Sukal, M. D. Ellis, J. P. Dewald, Shoulder abduction-induced reductions in reaching work area following hemiparetic stroke: Neuroscientific implications. *Exp. Brain Res.* 183, 215–223 (2007).
13. J. L. Boakes, J. Foran, S. R. Ward, R. L. Lieber, Muscle adaptation by serial sarcomere addition 1 year after femoral lengthening. *Clin. Orthop. Relat. Res.* 456, 250–253 (2007).
14. R. Csapo, C. N. Maganaris, O. R. Seynnes, M. V. Narici, On muscle, tendon and high heels. *J. Exp. Biol.* 213, 2582–2588 (2010).
15. B. R. Eisenberg, J. M. Brown, S. Salmons, Restoration of fast muscle characteristics following cessation of chronic stimulation. The ultrastructure of slow-to-fast transformation. *Cell Tissue Res.* 238, 221–230 (1984).
16. D. Kernell, Y. Donselaar, O. Eerbeek, Effects of physiological amounts of high- and low-rate chronic stimulation on fast-twitch muscle of the cat hindlimb. II. Endurance-related properties. *J. Neurophysiol.* 58, 614–627 (1987).
17. D. Kernell, O. Eerbeek, B. A. Verhey, Y. Donselaar, Effects of physiological amounts of high- and low-rate chronic stimulation on fast-twitch muscle of the cat hindlimb. I. Speed- and force-related properties. *J. Neurophysiol.* 58, 598–613 (1987).
18. P. E. Williams, G. Goldspink, The effect of immobilization on the longitudinal growth of striated muscle fibres. *J. Anat.* 116, 45–55 (1973).
19. D. B. Thomason, R. E. Herrick, D. Surdyka, K. M. Baldwin, Time course of soleus muscle myosin expression during hindlimb suspension and recovery. *J Appl Physiol (1985)* 63, 130–137 (1987).
20. C. Gans, W. J. Bock, The functional significance of muscle architecture—A theoretical analysis. *Ergeb. Anat. Entwicklungsgesch.* 38, 115–142 (1965).
21. R. L. Lieber, J. Fridén, Functional and clinical significance of skeletal muscle architecture. *Muscle Nerve* 23, 1647–1666 (2000).
22. C. Gans, Fiber architecture and muscle function. *Exerc. Sport Sci. Rev.* 10, 160–207 (1982).
23. R. D. Sacks, R. R. Roy, Architecture of the hind limb muscles of cats: Functional significance. *J. Morphol.* 173, 185–195 (1982).
24. R. L. Lieber, *Skeletal Muscle Structure, Function & Plasticity: The Physiological Basis of Rehabilitation* (Lippincott Williams & Wilkins, Philadelphia, PA, ed. 2, 2002).
25. F. E. Zajac, Muscle and tendon: Properties, models, scaling, and application to biomechanics and motor control. *Crit. Rev. Biomed. Eng.* 17, 359–411 (1989).
26. P. L. Powell, R. R. Roy, P. Kanim, M. A. Bello, V. R. Edgerton, Predictability of skeletal muscle tension from architectural determinations in guinea pig hindlimbs. *J. Appl. Physiol.* 57, 1715–1721 (1984).
27. W. M. Murray, T. S. Buchanan, S. L. Delp, The isometric functional capacity of muscles that cross the elbow. *J. Biomech.* 33, 943–952 (2000).
28. P. E. Williams, G. Goldspink, Changes in sarcomere length and physiological properties in immobilized muscle. *J. Anat.* 127, 459–468 (1978).
29. P. E. Williams, G. Goldspink, Longitudinal growth of striated muscle fibres. *J. Cell Sci.* 9, 751–767 (1971).
30. J. C. Tabary, C. Tabary, C. Tardieu, G. Tardieu, G. Goldspink, Physiological and structural changes in the cat's soleus muscle due to immobilization at different lengths by plaster casts. *J. Physiol.* 224, 231–244 (1972).
31. M. A. Mathewson, S. R. Ward, H. G. Chambers, R. L. Lieber, High resolution muscle measurements provide insights into equinus contractures in patients with cerebral palsy. *J. Orthop. Res.* 33, 33–39 (2015).
32. R. L. Lieber, J. Fridén, Muscle contracture and passive mechanics in cerebral palsy. *J Appl Physiol (1985)* 126, 1492–1501 (2019).
33. M. A. Mathewson, R. L. Lieber, Pathophysiology of muscle contractures in cerebral palsy. *Phys. Med. Rehabil. Clin. N. Am.* 26, 57–67 (2015).
34. A. M. Gordon, A. F. Huxley, F. J. Julian, The variation in isometric tension with sarcomere length in vertebrate muscle fibres. *J. Physiol.* 184, 170–192 (1966).
35. R. L. Lieber, W. M. Murray, D. L. Clark, V. R. Hentz, J. Fridén, Biomechanical properties of the brachioradialis muscle: Implications for surgical tendon transfer. *J. Hand Surg. Am.* 30, 273–282 (2005).
36. W. M. Murray, V. R. Hentz, J. Fridén, R. L. Lieber, Variability in surgical technique for brachioradialis tendon transfer. Evidence and implications. *J. Bone Joint Surg. Am.* 88, 2009–2016 (2006).
37. M. E. Llewellyn, R. P. J. Barretto, S. L. Delp, M. J. Schnitzer, Minimally invasive high-speed imaging of sarcomere contractile dynamics in mice and humans. *Nature* 454, 784–788 (2008).
38. G. N. Sanchez et al., In vivo imaging of human sarcomere twitch dynamics in individual motor units. *Neuron* 88, 1109–1120 (2015).
39. F. Gao, L.-Q. Zhang, Altered contractile properties of the gastrocnemius muscle poststroke. *J Appl Physiol (1985)* 105, 1802–1808 (2008).
40. J. W. Ramsay, T. S. Buchanan, J. S. Higginson, Differences in plantar flexor fascicle length and pennation angle between healthy and poststroke individuals and implications for poststroke plantar flexor force contributions. *Stroke Res. Treat.* 2014, 919486 (2014).
41. C. English, H. McLennan, K. Thoirs, A. Coates, J. Bernhardt, Loss of skeletal muscle mass after stroke: A systematic review. *Int. J. Stroke* 5, 395–402 (2010).
42. J. W. Ramsay, P. J. Barrance, T. S. Buchanan, J. S. Higginson, Paretic muscle atrophy and non-contractile tissue content in individual muscles of the post-stroke lower extremity. *J. Biomech.* 44, 2741–2746 (2011).
43. N. Metoki, Y. Sato, K. Satoh, K. Okumura, J. Iwamoto, Muscular atrophy in the hemiplegic thigh in patients after stroke. *Am. J. Phys. Med. Rehabil.* 82, 862–865 (2003).
44. F. E. Zajac, How musculotendon architecture and joint geometry affect the capacity of muscles to move and exert force on objects: A review with application to arm and forearm tendon transfer design. *J. Hand Surg. Am.* 17, 799–804 (1992).
45. A. S. Ryan, C. L. Dobrovolny, G. V. Smith, K. H. Silver, R. F. Macko, Hemiparetic muscle atrophy and increased intramuscular fat in stroke patients. *Arch. Phys. Med. Rehabil.* 83, 1703–1707 (2002).
46. L. Li, K. Y. Tong, X. Hu, The effect of poststroke impairments on brachialis muscle architecture as measured by ultrasound. *Arch. Phys. Med. Rehabil.* 88, 243–250 (2007).
47. C. M. Nelson, W. M. Murray, J. P. A. Dewald, Motor impairment-related alterations in biceps and triceps brachii fascicle lengths in chronic hemiparetic stroke. *Neurorehabil. Neural Repair* 32, 799–809 (2018).
48. L. R. P. Garmirian, A. M. Acosta, R. Schmid, J. P. A. Dewald, Volume and intramuscular fat content of upper extremity muscles in individuals with chronic hemiparetic stroke. *bioRxiv* [Preprint] (2019). https://doi.org/10.1101/687699 (Accessed 2 July 2020).
49. M. Y. Bhadane, F. Gao, G. E. Francisco, P. Zhou, S. Li, Correlation of resting elbow angle with spasticity in chronic stroke survivors. *Front. Neurol.* 6, 183 (2015).
50. K. R. Holzbaur, W. M. Murray, G. E. Gold, S. L. Delp, Upper limb muscle volumes in adult subjects. *J. Biomech.* 40, 742–749 (2007).
51. T. Fukunaga et al., Muscle volume is a major determinant of joint torque in humans. *Acta Physiol. Scand.* 172, 249–255 (2001).
52. H. S. Im, K. E. Alter, S. Brochard, C. Pons, F. T. Sheehan, In vivo pediatric shoulder muscle volumes and their relationship to 3D strength. *J. Biomech.* 47, 2730–2737 (2014).
53. Y. Lan, J. Yao, J. P. A. Dewald, The impact of shoulder abduction loading on volitional hand opening and grasping in chronic hemiparetic stroke. *Neurorehabil. Neural Repair* 31, 521–529 (2017).
54. L. R. Smith, K. S. Lee, S. R. Ward, H. G. Chambers, R. L. Lieber, Hamstring contractures in children with spastic cerebral palsy result from a stiffer extracellular matrix and increased in vivo sarcomere length. *J. Physiol.* 589, 2625–2639 (2011).
55. L. Ada, C. G. Canning, S. L. Low, Stroke patients have selective muscle weakness in shortened range. *Brain* 126, 724–731 (2003).
56. T. L. Wickiewicz, R. R. Roy, P. L. Powell, V. R. Edgerton, Muscle architecture of the human lower limb. *Clin. Orthop. Relat. Res.* 275–283 (1983).
57. T. Fukunaga et al., Physiological cross-sectional area of human leg muscles based on magnetic resonance imaging. *J. Orthop. Res.* 10, 928–934 (1992).
58. T. D. O'Brien, N. D. Reeves, V. Baltzopoulos, D. A. Jones, C. N. Maganaris, In vivo measurements of muscle specific tension in adults and children. *Exp. Physiol.* 95, 202–210 (2010).
59. C. I. Morse, J. M. Thom, N. D. Reeves, K. M. Birch, M. V. Narici, In vivo physiological cross-sectional area and specific force are reduced in the gastrocnemius of elderly men. *J. Appl. Physiol. (1985)* 99, 1050–1055 (2005).
60. K. R. S. Holzbaur, W. M. Murray, S. L. Delp, A model of the upper extremity for simulating musculoskeletal surgery and analyzing neuromuscular control. *Ann. Biomed. Eng.* 33, 829–840 (2005).
61. A. Rajagopal et al., Full-body musculoskeletal model for muscle-driven simulation of human gait. *IEEE Trans. Biomed. Eng.* 63, 2068–2079 (2016).
62. R. R. Roy, I. D. Meadows, K. M. Baldwin, V. R. Edgerton, Functional significance of compensatory overloaded rat fast muscle. *J. Appl. Physiol.* 52, 473–478 (1982).

Adkins et al.
Serial sarcomere number is substantially decreased within the paretic biceps brachii in individuals with chronic hemiparetic stroke

63. S. A. Spector, P. F. Gardiner, R. F. Zernicke, R. R. Roy, V. R. Edgerton, Muscle architecture and force-velocity characteristics of cat soleus and medial gastrocnemius: Implications for motor control. *J. Neurophysiol.* **44**, 951–960 (1980).

64. M. E. Vidt *et al.*, Characterizing upper limb muscle volume and strength in older adults: A comparison with young adults. *J. Biomech.* **45**, 334–341 (2012).

65. C. M. Nelson, J. P. A. Dewald, W. M. Murray, In vivo measurements of biceps brachii and triceps brachii fascicle lengths using extended field-of-view ultrasound. *J. Biomech.* **49**, 1948–1952 (2016).

66. M. Takahashi, S. R. Ward, L. L. Marchuk, C. B. Frank, R. L. Lieber, Asynchronous muscle and tendon adaptation after surgical tensioning procedures. *J. Bone Joint Surg. Am.* **92**, 664–674 (2010).

67. M. D. Ellis, B. G. Holubar, A. M. Acosta, R. F. Beer, J. P. A. Dewald, Modifiability of abnormal isometric elbow and shoulder joint torque coupling after stroke. *Muscle Nerve* **32**, 170–178 (2005).

68. S. S. M. Lee, S. Spear, W. Z. Rymer, Quantifying changes in material properties of stroke-impaired muscle. *Clin. Biomech. (Bristol, Avon)* **30**, 269–275 (2015).

69. L. Weng *et al.*, US extended-field-of-view imaging technology. *Radiology* **203**, 877–880 (1997).

70. A. N. Adkins, P. W. Franks, W. M. Murray, Demonstration of extended field-of-view ultrasound's potential to increase the pool of muscles for which in vivo fascicle length is measurable. *J. Biomech.* **63**, 179–185 (2017).

71. J. M. Elliott *et al.*, Magnetic resonance imaging findings of fatty infiltrate in the cervical flexors in chronic whiplash. *Spine* **35**, 948–954 (2010).

72. C. P. Elder, D. F. Apple, C. S. Bickel, R. A. Meyer, G. A. Dudley, Intramuscular fat and glucose tolerance after spinal cord injury–A cross-sectional study. *Spinal Cord* **42**, 711–716 (2004).

73. J. Schindelin *et al.*, Fiji: An open-source platform for biological-image analysis. *Nat. Methods* **9**, 676–682 (2012).

74. J. Elliott, D. Walton, A. Rademaker, T. Parrish, Quantification of cervical spine muscle fat: A comparison between T1-weighted and multi-echo gradient echo imaging using a variable projection algorithm (VARPRO). *BMC Med. Imaging* **13**, 30 (2013).

75. A. Smith *et al.*, Muscle-Fat MRI: 1.5 Tesla and 3.0 tesla versus histology. *Muscle Nerve* **50**, 170–176 (2014).

Adkins et al.
Serial sarcomere number is substantially decreased within the paretic biceps brachii in individuals with